Interpretation of the Partial Coalescence Prior to Rupture Using Riedel's Cavitation Model Based on Qualitative Cavity Shape Data

Mohamed Abdelrehim and Qiang Xu

August 3, 2024

Interpretation of the Partial Coalescence Prior to Rupture Using Riedel's Cavitation Model Based on Qualitative Cavity Shape Data

Mohamed Abdelrehim
University of Huddersfield
Huddersfield, UK
mohamedhassan.abdelrehim@hud.ac.uk

Qiang Xu
University of Huddersfield
Huddersfield, UK
q.xu2@hud.ac.uk

***Abstract*— Studying the creep cavitation damage where cavities form, nucleate, grow, and coalesce along the grain boundaries is one way forward to predict the lifetime of materials susceptible to creep deformation in industrial applications such as power plants, where elevated temperatures are paramount. Although Riedel's generic cavitation equations existed since 1990, the cavitation models were calibrated when the calibration method was designed in 2017 by the second author. The existing models assume no partial coalescence. Here, we will move forward to take the partial coalescence prior to rupture to calibrate the nucleation and cavity growth using a specific cavity shape. The cavity shape seems to provide useful qualitative data, facilitating the comprehension of the partial coalescence mechanism with the aid of the current cavitation model. The specific material and creep test we investigated is brass alloy Cu–40Zn–2Pb microtomography. Focusing only on the complex shapes having a complexity factor above 0.75, where the coalescence has been evidently associated with such shapes, the current model can be applied to further understand the mechanism at creep times ranging from 137 minutes to 440 minutes. This is done by interpreting the number of cavities and the size of the cavities before and after the coalescence. A complex cavity shape is a result of the coalescence between multiple spherical cavity shapes. The increasing nucleation rate and the decreasing growth rate have been significantly associated with the coalescence mechanism prior to rupture.**

I. Introduction

It is crucial to understand creep deformation of components in high-temperature industries like power generation and aerospace, where efficiency in operation is necessary [1]. Creep is a time-dependent deformation under static load and temperature. It involves three stages: primary, secondary, and tertiary, each influenced by different mechanisms. Microstructurally, creep cavitation damage initiates from the earliest stages of deformation, often invisible to the naked eye, progressing until fracture occurs, which can be visually found in critical components. Although the transition time between these stages varies depending on the microstructural response to different creep mechanisms, cavitation damage is inevitable. It predominantly occurs along grain boundaries and triple junctions as cavities form, nucleate, grow, and coalesce over time.

Experimentally, Synchrotron tomography techniques (X-ray), revealing cavitation data can be employed to develop models for creep rupture [2]. It represents the data in a three-dimensional view, showcasing the chronological sequence of microstructural damage [3]. One approach of modelling these data is the continuum damage mechanics. It depicts creep rupture time associated with cavitation mechanisms [4], [5], [6], [7], [8]. Thus, quantifying the resulting cavitation damage evolution with time enables the modelling and the prediction of creep lifetime [9]. Qiang Xu calibrated Riedel's cavitation model, introducing a method, demonstrating its effectiveness in representing cavitation data and predicting nucleation and growth cavitation behavior in real-time. The method for calibration and modelling was latter developed by Xu and others [10] [11]. The use of exact cavity diameters rather than averages and the association between the cavitation damage and the wide stress levels distinguish this model. Riedel's model includes equations for nucleation rate, growth rate, and cavity size distribution but ignores the coalescence mechanism, despite its significant role in the late stages of rupture in creep cavitation [12] [13] [14]. It assumes only spherical cavity shapes, while observed cavity shapes in previous in-situ tomographic investigations were not limited to spheres but rather took different shape [15] [16], [17]. Recent developments on the current cavitation model showed slight deviation in the total volume during the late stages suggesting the predominance of coalescence [18].

The objective of this study is to apply the current cavitation model using specific cavity shapes, with a focus on the brass alloy Cu–40Zn–2Pb microtomography, by analyzing only cavity shapes that are formed due to coalescence. This paper utilizes the current model to understand the mechanism of partial coalescence and interpret the number and size of cavities before and after coalescence to provide insights into this phenomenon. The study is limited to the brass alloy Cu–40Zn–2Pb, and future work will explore a broader range of materials to test the model's applicability and robustness across different contexts. Additionally, exploring the quantitative impact of coalescence on material properties like strength and ductility can provide more actionable insights for material engineers. This paper builds upon existing methodologies, refining the understanding of coalescence mechanisms by incorporating partial coalescence effects, and aims to advance the modelling of creep cavitation damage in high-temperature industrial applications.

II. Purpose

(1) Apply the current cavitation model using specific cavity shapes, with a focus on the brass alloy Cu–40Zn–2Pb microtomography, by analyzing only cavity shapes that are formed due to coalescence. The paper utilizes the current model to understand the mechanism of partial coalescence. The study is limited to the brass alloy Cu–40Zn–2Pb. Future work will explore a broader range of materials to test the model's applicability and robustness across different contexts.

(2) Interpret the number and size of cavities before and after coalescence to provide insights into this phenomenon.

III. PARTIAL COALESCENCE CAVITY SHAPE CHARACTERISTICS

Cavities form, nucleate, grow, and coalesce along grain boundaries and triple junctions leading to microcracks, macrocracks, and fractures. Classifying cavity shapes over time during creep can indicate the dominant cavitation mechanism. The increasing strain driven by super-plasticity and grain boundary sliding have been associated with irregular cavity shapes indicating coalescence. [19]. Under high stress levels, cavities transition from equiaxed to larger, rod-shaped forms, accelerating growth and coalescence, ultimately resulting in micro-cracks. [20] . A study on P91 steel proposed a coalescence threshold for cavity area of approximately 5 mm2, marking the transition from void nucleation and growth to coalescence [21]. Cavity shape classification during in-situ 3D microtomographic assessment on the brass alloys showed that complex cavity shapes are resulting from coalescence, where these shapes have a complexity factor of above 0.75. The study showed that a complexity factor above 0.75 is an indication of coalescence [17]. However, cavities with broad interconnecting bridges previously reported in the E911 study were non-coalesced and yet had a complexity factor above 0.75. Alternatively, cavity elongation provided a critical value of 1.9 to distinguish between coalesced and non-coalesced cavities [23]. Previous observations suggest that cavity coalescence can be indicated by multiple factors. Three approaches can be utilised to describe the coalescence mechanism, which are the strain effect, the grain boundary mechanism effect, and the cavity shape indicators, including the complexity factor and the elongation. Analyzing cavity shape offers a direct method for understanding the coalescence mechanism, where critical values for shape are provided. Qualitatively, complex shapes data revealing their total number of cavities and their total volume evolutions with creep time had been found in previous brass alloy study [17]. No similar data for only elongated shapes with elongations above 1.9 to provide the total number of cavities and total volume evolutions was found. It should be noted that, quantitatively, the evolution of cavity elongation and its relationship with size may further provide an adequate description for the coalescence. This would require a more extensive investigation, which can be presented in a separate study. Therefore, to comprehend the coalescence mechanism, this study suggests employing qualitative data on complex cavity shapes as a straightforward approach.

IV. CAVITATION MODEL

Riedel (1986) [24] proposed a function, N (R, t), to describe their size distribution at specific creep times. The original model introduced power-law expressions incorporating both cavity growth rate and nucleation. Xu, et.al [7] [8] calibrated and developed the model to describe total cavitation damage during creep. Their work established methods for determining constants, characterizing size distribution, and integrating nucleation and growth rates. This facilitated the description the of individual (non-coalesced) cavity growth, the total number of cavities, size distribution, and the total cavitation damage at specific creep times. The developed model describes the exact cavity sizes without relying on average values, which provides an advantage for modelling the creep cavitation damage across both short- and long-term creep durations. However, late-stage cavity coalescence was ignored by the original model.

$$(t_f) = A_2\left(t_f^{\gamma+1} - t_0^{\gamma+1}\right)/(\gamma+1) \qquad (1.0)$$

The corresponding cavity radius R for each creep time t can be found by substituting the obtained growth rate constants from step.1 in the integrated growth rate [7], [8], where the cavity radius R can be written as,

$$R = \left((\beta+1)(A_1 \ln t + C)\right)^{\frac{1}{\beta+1}} \qquad (2.0)$$

Cavity Size Distribution Function at a Specific Creep Time N(R,t): Displays the frequency of each cavity size at a specific creep time for a range of cavity sizes due to nucleation and growth. It aims to describe the experimental histogram.

$$N(R, t_f) = (A_2/A_1)R^{\beta} t_f^{1+\gamma} \exp\left(-(\gamma+1)R^{\beta+1}/A_1(\beta+1)\right) \qquad (3.0)$$

Total Cavitation Damage Total Volume

To numerically calculate the total volume V, the sum of the cavity volumes occupied by the individual cavities is multiplied by their density. The method was applied in [18].

$$\sum_{R(t_0)}^{R(t_f)} V(R) N(R,t)\, dR \qquad (4.0)$$

V. METHOD AND MATERIAL

Creep cavitation data, which is based on 3D in-situ x-synchrotron tomography performed on the brass alloy Cu-40Zn-2Pb for 440 minutes, has been selected [17]. Only the complex shapes resulting from cavity coalescence have been selected, along with the quantitative collection of the total number and volume of cavities of these shapes at specific creep times. Since the model describes non-coalesced individual cavities, the resulting number of cavities has been estimated by conserving the total volume from the model to match the one in the experiment. The reasons behind selecting this material are: (1) the comprehensiveness of the data where the cavity shape, cavity size, number of cavities, size distributions, and total volume is provided at different creep times; (2) other materials may provide cavitation data but may not be comprehensive or include the cavity shape change with time which is found to be an indicator for the coalescence mechanism. Furthermore, the study mainly focuses on providing and interpreting a method that can be applied to other materials if the cavitation data, including the cavity shape, is provided. The cavity sizes were converted from volumes represented in voxels to equivalent spherical cavity radii (R) represented in micro-meters (µm), with each voxel corresponding to a volume of 1.63 cubic micro-meters (µm^3). Excel equation solver has been used to perform the calculations for the values of the constants and the total number of cavities before the coalescence.

Using Riedel's model, the interpretation of the partial coalescence has been made based on the following steps: (1)

Set the initial values of constants as shown in (table .1). Constants can be obtained using a trial-and-error method base on total volume conservation. (2) Listing the creep times. The first creep times listed are 1, 1.5, and 2 minutes then increments of one-minute step were applied up to a specified creep time. This step is repeated for each specified creep time shown in table (1), for each size distribution. (3) Calculating the corresponding cavity size (radius) for each creep time, using the integrated growth rate equation (2.0). (4)

Calculate the total number of cavities based on equating the total volume of complex shapes in the experiment to the total volume in the model. The total volume of cavities of the model is calculated using the total volume equation (4.0). The corresponding total number of cavities for each creep time, using the integrated nucleation rate equation (3.0).

The computed total number of cavities indicates the count of individual cavities that collectively formed the complex shapes representing coalesced cavities as shown in (table 2). This reveals the total number of cavities which before they coalesce.

VI. Results

Table 1: Nucleation rate Constants and growth rate constants

Time (minutes)	A_2	γ	A_1	β	C
52	1.06543	0.44	0.41631	0.1	0.9
110	1.70435	0.44	0.48972	0.1	0.9
137	2.27884	0.44	0.54920	0.1	0.9
196	3.08889	0.44	0.58455	0.1	0.9
307	8.77235	0.44	0.86600	0.1	0.9
333	10.3759	0.44	0.91436	0.1	0.9
361	13.0173	0.44	0.98893	0.1	0.9
389	16.3313	0.44	1.06959	0.1	0.9
416	20.3236	0.44	1.15358	0.1	0.9
440	24.6847	0.44	1.23377	0.1	0.9

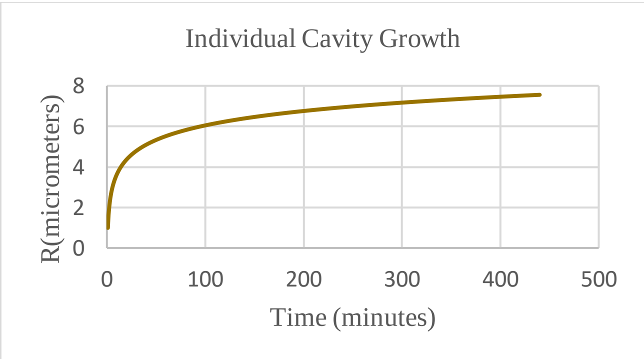

Figure 1: Individual Non-coalesced Cavity Growth (after 440 minutes)

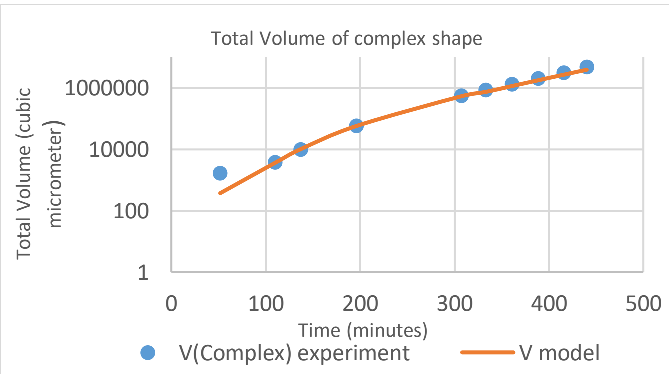

Figure 2: Total Cavitation Damage by coalescence (Total volume of complex cavities) evolution from 52 to 440 minutes.

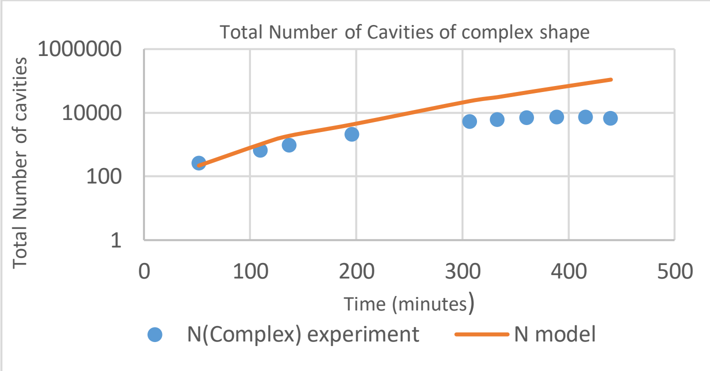

Figure 3: Evolution of Total number of Cavities before (model) and after (experiment) Coalescence from 52 to 440 minutes.

Table 2: The total number of cavities before (from the model) and after (from the experiment) coalescence.

Time (minutes)	Total number of cavities after coalescence	Total number of cavities before coalescence
52	268	219
110	668	1030
137	975	1889
196	2098	4288
307	5397	23240
333	6142	30901
361	6921	43548
389	7274	60839
416	7274	83393
440	6717	109807

VII. Interpretation of the Coalescence Mechanism

As shown in Table 1, the nucleation rate constant A2 and the growth rate constant A1 show an exponential increase with respect to creep time. However, the rate of increase in A2 is greater than that in A1. This means that A2 contributes more to the formation of total damage in complex shapes in comparison to A1. In Figure 2, the model represents the total volume of the non-coalesced cavities, while the experiment represents the same total volume of the coalesced cavities, which is identified by the complex shapes. Since both total volumes are conserved, knowing that the model considers non-coalesced cavities while the experiment considers coalesced cavities, the total number of cavities calculated by the model represents the number of cavities before the coalescence, while the number of complex shapes from the experiment represents the number of cavities after the coalescence. This can be illustrated in Figure 3, which reveals that the coalescence mechanism is driven by the increase in the nucleation rate. In Table 2, after 110 minutes, the number of cavities after coalescence is 668, which was formed by the coalescence of 1030 cavities. This difference between the number of cavities before and after coalescence increases with the increase in time. At 440 minutes, the number of cavities after the coalescence is 6717, which was formed by

109807 cavities before the coalescence. The consistency in the increase between the number of cavities before and after coalescence may assist in further modelling a probability for the coalescence to be added to the current cavitation model. Furthermore, with the aid of size distribution modelling, the size distribution of the cavities before and after coalescence can be modelled. It can be suggested that the coalescence mechanism is a result of the sudden increase in the number of cavities that is accompanied by a by a decrease in the growth rates of individual cavities

VIII. Conclusion

The study aimed to address the limitations of current cavitation models by incorporating partial coalescence prior to rupture, focusing on the brass alloy Cu–40Zn–2Pb microtomography. The model offers a precise understanding of coalescence describing individual cavity growth, total cavity number, size distribution, and total cavitation damage at specific creep times by analyzing complex cavity shapes resulting from coalescence. The increasing nucleation rate and decreasing growth rate associated with the coalescence mechanism prior to rupture, providing valuable insights for future work. The consistency observed in the increase between the number of cavities before and after coalescence suggests the potential for further modelling of coalescence probability in current cavitation models. Additionally, the analysis facilitates the modelling of size distribution, the size distribution of cavities before and after coalescence. It can be further suggested that coalescence is more likely driven by the nucleation rate increase. This coalescence mechanism impacts material properties by forming microcracks that evolve into macrocracks. This progression affects the material's ductility, transitioning it from a ductile to a brittle state prior to fracture.

References

[1] R. Viswanathan ,K. Coleman, U. Rao , "Materials for ultra-supercritical coal-fired power plant boilers," International Journal of Pressure Vessels and Piping, pp. 778-783, 2006. [2] R. KUMAR, "In situ nanotomography investigation of cavity nucleation and growth in light alloys during high temperature deformation," THE GRENOBLE ALPES UNIVERSITY , 2016. [3] A. Isaac, F. Sket, W. Reimers, B. Camin, G. Sauthoff, A.R. Pyzalla, "In situ 3D quantification of the evolution of creep cavity size, shape, and spatial orientation using synchrotron X-ray tomography," Materials Science and Engineering, pp. 108-118, 2007. [4] C. Phaniraj, B.K. Choudhary, K. Bhanu Sankara Rao, Baldev Raj, "Relationship between time to reach Monkman–Grant ductility and rupture life," Scripta Materialia, pp. 1313-1318, 2003. [5] Mohammad Shafinul Haque, Calvin Maurice Stewart, "Comparative analysis of the sin-hyperbolic and Kachanov–Rabotnov creep-damage models," International Journal of Pressure Vessels and Piping, pp. 1-9, 2019. [6] Qiang Xu and Zhongyu Lu, "Modeling of Creep Deformation and Creep Fracture," Strength of Materials, 2019. [7] Qiang Xu, Xin Yang & Zhongyu Lu, "On the development of creep damage constitutive equations: a modified hyperbolic sine law for minimum creep strain rate and stress and creep fracture criteria based on cavity area fraction along grain boundaries," Materials at High Temperatures, pp. 323-332, 2017. [8] Xuming Zheng, Qiang Xu, Zhongyu Lu, Xue Wang & XiQiao Feng, "The development of creep damage constitutive equations for high Cr steel," Materials at High Temperatures, pp. 129-138, 2020. [9] Xu, Qiang, Zhongyu Lu, and Xue Wang, "Damage modelling: the current state and the latest progress on the development of creep damage constitutive equations for high Cr steels.," Materials at High Temperatures, 2017. [10] Zheng, X. et al., "The development of creep damage constitutive equations for high Cr steel," Materials at High Temperatures, pp. 129-138, 2020. [11] X. Zheng, "The development and application of creep damage constitutive equations for high Cr steels over a wide range of stress," University of Huddersfield Repository, 2021. [12] K. Valliappa, "Creep, Fatigue and Cr atigue and Creep-Fatigue Inter atigue Interactions in Modified 9% Cr -1% Mo (P91) Steels," University of Arkansas, pp. 18, 30, 93, 94, 2013. [13] V. Sklenička, K. Kuchařová, M. Svoboda, L. Kloc, J. Buršık, A. Kroupa, "Long-term creep behavior of 9–12%Cr power plant steels," Materials Characterization, pp. 38-39, 2003. [14] X. Yang, "The Development of Creep Damage Constitutive Equations for High Chromium Steel Based on the Mechanism of Cavitation Damage," University of Huddersfield Repository, pp. 55-59, 2018. [15] Borbély, A., Dzieciol, K., Sket, F. et al, "Characterization of creep and creep damage by in-situ microtomography," the journal of the Minerals, Metals & Materials Society, p. 81, 2011. [16] Isaac, A., Dzieciol, K., Sket, F. et al. , "In-Situ Microtomographic Characterization of Single-Cavity Growth During High-Temperature Creep of Leaded Brass," Metall Mater Trans, pp. 3025-3027, 2011. [17] A. Isaac, F. Sket, W. Reimers, B. Camin, G. Sauthoff, A.R. Pyzalla, "In situ 3D quantification of the evolution of creep cavity size, shape, and spatial orientation using synchrotron X-ray tomography," Materials Science and Engineering, pp. 108-118, 2007. [18] Mbombo Amejima OKPA, Qiang XU, Zhongyu LU, "The Development of the Cavitated Volume Fraction as a Creep Damage Indicator for Creep Remnant Life Prediction," School of Computing and Engineering, University of Huddersfield, pp. 3-10, 2023. [19] C.F Martin, C Josserond, L Salvo, J.J Blandin, P Cloetens, E Boller, "Characterisation by X-ray micro-tomography of cavity coalescence during superplastic deformation," Scripta Materialia, pp. 375-381, 2000. [20] Yunhe Yu, Zhengdong Liu, Chi Zhang, Zhongding Fan, Zhengzong Chen, Hansheng Bao, Hao Chen, Zhigang Yang, "Correlation of creep fracture lifetime with microstructure evolution and cavity behaviors in G115 martensitic heat-resistant steel," Materials Science and Engineering: A, pp. 1-8, 2020. [21] Ke Han, Haimin Ding, Xiaoliang Fan, Wenbin Li, Yadong Lv, Yanting Feng, "Study of the creep cavitation behavior of P91 steel under different stress states and its effect on high-temperature creep properties," Journal of Materials Research and Technology, pp. 47-59, 2022.